Measuring the remanent magnetic moment of a kilogram-level test mass for TianQin

Jia-Hao Xu,[1,2] Qi Liu,[2,*] and Lin Zhu[3]

[1]Faculty of Information Engineering, Quzhou College of Technology, Quzhou, 324000, China
[2]MOE Key Laboratory of TianQin Mission, TianQin Research Center for Gravitational Physics and School of Physics and Astronomy, Frontiers Science Center for TianQin, Gravitational Wave Research Center of CNSA, Sun Yat-sen University (Zhuhai Campus), Zhuhai 519082, China
[3]MOE Key Laboratory of Fundamental Physical Quantities Measurement, Hubei Key Laboratory of Gravitation and Quantum Physics, PGMF and School of Physics, Huazhong University of Science and Technology, Wuhan 430074, China

(Received 23 May 2024; accepted 5 August 2024; published 3 September 2024)

In the TianQin space-based gravitational wave (GW) detection mission, the measurement of remanent magnetic moment ($\vec{m}$) of the kilogram-level test mass is a prerequisite before the launch. Current measurement methods have shown a measured deviation since the assumption of a uniform distribution of $\vec{m}$ in the test mass volume, and the unconsidered interference from ambient magnetic fields. We develop a new torsion pendulum with a modulated 2D Helmholtz coils to measure the $\vec{m}$. The 2D Helmholtz coils are set to get rid of the assumption and avoid the undesired systematic interference. The measurement precision of $\vec{m}$ by our instrument is better than 1 nA m^2. The instrument is particularly useful for measuring the extremely low magnetic properties of the materials for use in the construction of TianQin space-based GW detection and other precision scientific apparatus.

DOI: 10.1103/PhysRevD.110.062001

I. INTRODUCTION

An isolated metal test mass (TM) in a time-varying magnetic field will sense a magnetic force, which is a crucial noise source in almost all space-based precision missions that use the TM as the central sensitive probe [1–6]. In the TianQin space-based GW detection mission, the low-frequency sensitivity is limited by residual accelerations of its caged kg-level alloy TM cube [7]. The magnetic force noise is one of largest contributor of the residual accelerations (magnetic noise budget flowdown: 24%). Fluctuations in the magnetic field lead to residual accelerations of the TM. The primary force derived from remanent magnetic moment $\vec{m}$ of the TM couple with the time-varying interplanetary magnetic field. The remanent permanent magnetic moment $\vec{m}$ is the total of permanent magnetization $\vec{M}(\vec{r})$ in TM volume element dV at $\vec{r}$, and can be quantified by

$$\vec{m} = \int \vec{M}(\vec{r}) dV. \tag{1}$$

TianQin requires the $|\vec{m}|$ less than 10 nA m^2. For verifying the very stringent cleanliness and improving the magnetic-related baseline design of spacecrafts, it is prerequisite to precisely determine the $\vec{m}$, with a required measurement resolution level 1 nA m^2 in TianQin GW detection missions [8–10].

Some methods based on torsion pendulum were developed to measure the $\vec{m}$ [8,11–14]. The basic idea of these methods is similar. The coils are set around the TM suspended by a fiber. The artificial field $\vec{B}(\vec{r})$ originated from coils is applied to the permanent magnetization $\vec{M}(\vec{r})$ per unit volume dV. Then, the $\vec{m}$-related torque [15]

$$\vec{\tau} = \int \vec{M}(\vec{r}) \times \vec{B}(\vec{r}) dV + \int \vec{r} \times [\vec{M}(\vec{r}) \cdot \nabla] \vec{B}(\vec{r}) dV \tag{2}$$

apply to the torsion pendulum. Assuming the uniform distribution of permanent magnetization $\vec{M}(\vec{r})$ in the TM volume, the condition $\vec{M}(\vec{r}) \equiv \vec{m}/V$ can be obtained. Then the Eq. (2) can be simply written as $\vec{\tau} = \frac{1}{V} \int \vec{m} \times \vec{B}(\vec{r}) + \vec{r} \times (\vec{m} \cdot \nabla) \vec{B}(\vec{r}) dV$. Combine the assumption, the measured $\vec{\tau}$ and the known $\vec{B}(\vec{r})$, then the $\vec{m}$ can be measured. However, the assumption in these methods could not be warranted, since the distribution of $\vec{M}(\vec{r})$ is generally random due to the imperfect composition, heat and mechanical treatment of the alloy TM [16,17]. The assumption will contribute to a measured deviation. For instance, if the $\vec{M}(\vec{r})$ mainly distribute in TM volume elements close to the coils where the strong gradient of $\vec{B}(\vec{r})$ exists, then the value $\vec{m}$ measured by these methods will overestimate the actual value.

*Contact author: liuq239@sysu.edu.cn

On the other hand, the ambient laboratory magnetic fields $\vec{B}_a(\vec{r})$ will add to the $\vec{B}(\vec{r})$ and hence contribute to a systematic noise. Yin *et al.* assessed the impact of the geomagnetic field and added two extra coils to counteract its effect. However, a deviation still exists [12,14]. Hueller *et al.* adopted the modulated $\vec{B}(\vec{r})$ at frequency ω to separate the interference of $\vec{B}_a(\vec{r})$. But, the modulated method will produce some additional induced magnetic moment interference, and later cause measured $\vec{m}$ depends on the modulated ω. A brief illustration of the frequency dependence is mentioned in the measurement principle section, since a part of our instrument is based on Hueller's work [8].

In this paper, the principle of the novel measurement of the $\vec{m}$ is illustrated in Sec. II, and the instrument implementation is introduced in Sec. III. The measurement and results are reported in Sec. IV. The measured $\vec{m}$ of TMs are discussed in Sec. V, and a summary is presented in Sec. VI.

II. EXPERIMENTAL PRINCIPLE

A schematic of our core setup is shown in Fig. 1. The 2D Helmholtz coils are symmetrically placed around the TM. The magnetic field at $\vec{r}$ in TM is the superposition of the coils magnetic field $\vec{B}(\vec{r})$ and ambient magnetic field $\vec{B}_a(\vec{r})$. The dominant component of $\vec{B}_a(\vec{r})$ is the geomagnetic field, since the winding and framework of 2D Helmholtz coils close to TM are nonmagnetic aluminum and copper respectively. Thanks to the spatial uniformity property of the geomagnetic field and coils' magnetic field, the total field is uniform in the volume of the TM. Then, the gradient of the magnetic field approaches zero, and hence $[\vec{M}(\vec{r})\cdot\nabla]\vec{B}(\vec{r})\simeq 0$ in Eq. (2). It overcomes the assumption

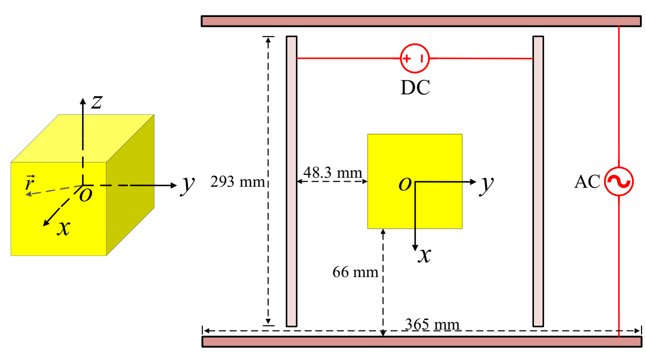

FIG. 1. Schematic diagram of the core setup. Left: the yellow cube represents the TM. The origin of the coordinate system, denoted as O, is at the center of TM. The horizontal axes x and y are perpendicular to the sides of the TM, and the z is parallel to the fiber. Right: the 2D Helmholtz coils are set around the TM. The axes of 2D Helmholtz coils coincide with the horizontal dimension x and y. The input currents of the Helmholtz coils along the x and y are DC (constant current) and AC (alternating current) respectively. The practical power sources for inputting to 2D Helmholtz coils are set about 5 m away from the TM.

of the uniform distribution of $\vec{M}(\vec{r})$, and Eq. (2) can be simplified as [18]

$$\vec{\tau} = \int \vec{M}(\vec{r}) \times \vec{B}(\vec{r}) dV. \tag{3}$$

The magnetic field in all TM elements along the x axis B_x can be set as $B_x(\vec{r}) = B_{cx}\sin(\omega t) + B_{ax}$, where the B_{cx} and ω are the amplitude and frequency of the x-axis coils AC field, and the B_{ax} is x-component of the $\vec{B}_a$. Similarly, the magnetic field in all TM elements along the y axis B_y can be set as $B_y(\vec{r}) = B_{cy} + B_{ay}$, where B_{cy} is the amplitude of the y-axis coils DC field, and the B_{ay} is y-component of the $\overrightarrow{B_a}$. According to Eq. (3), the $\vec{m}$-related torque along the z axis can be expressed as

$$\begin{aligned}\tau_z &= \int M_x(\vec{r})B_y(\vec{r}) - M_y(\vec{r})B_x(\vec{r})dV \\ &= (B_{cy} + B_{ay})\int M_x(\vec{r})dV \\ &\quad - [B_{cx}\sin(\omega t) + B_{ax}]\int M_y(\vec{r})dV \\ &= (B_{cy} + B_{ay})m_x - [B_{cx}\sin(\omega t) + B_{ax}]m_y \end{aligned}\tag{4}$$

where the $M_x(\vec{r})$, $M_y(\vec{r})$ are the x- and y-component of the $\vec{M}(\vec{r})$ respectively. The $m_x = \int M_x(\vec{r})dV$ and $m_y = \int M_y(\vec{r})dV$ are the horizontal components of the $\vec{m}$ with the assumption of uniform distribution.In this way, the m_y related torque is modulated at ω without the impact of the constant ambient field B_{ax} and B_{ay}. Based on the modulated $\tau_z(\omega) = B_{cx}m_y\sin(\omega t)$ in Eq. (4), the m_y can be measured. It is the basic principle of measurement of Hueller's work [8].

However, the coil and ambient magnetic field will induce TM to produce magnetic moment. That is to say, the magnetic moments in TM include the induced magnetic moment and the m. The additional induced magnetic moment interference should be considered in Eq. (4). The induced magnetic moment m' along the x and y can be written as $m'_x = [\chi_x(\omega)B_{cx}\sin(\omega t) + \chi_x(0)B_{ax}]V\mu_0^{-1}$ and $m'_y = \chi_y(0)(B_{cy} + B_{ay})V\mu_0^{-1}$ respectively, where χ is the volume-averaged susceptibility of the TM, V is the volume of TM. The $\chi(\omega)$ and $\chi(0)$ characterize the different induced intensity of TM in AC and DC magnetic field separately. The subscript x and y denote the different induced directions. Analogously, the m'-related torque along the z can be expressed as $\tau'_z = (B_{cy} + B_{ay})m'_x - [B_{cx}\sin(\omega t) + B_{ax}]m'_y$. The amplitude of time-varying torque $\tau'_z + \tau_z$ at ω can be written as

$$\overline{\tau}_z = B_{cx}[\chi_x(\omega) - \chi_y(0)](B_{cy} + B_{ay})V\mu_0^{-1} - B_{cx}m_y. \tag{5}$$

For the kilogram-level TM, the difference between the low-frequency $\chi(\omega)$ and the $\chi(0)$ about 1×10^{-5}, and this difference should be considerable [19,20]. Since the term $\chi_x(\omega)-\chi_y(0)\neq 0$, the measured m_y from the $\bar{\tau}_z$ are disturbed by the ambient B_{ay}, and the measured m_y are different under different modulated frequency ω. We adopt a Helmholtz coils magnetic field B_{cy} to compensate the ambient B_{ay}, namely, $B_{cy}+B_{ay}=0$. Then, the interference from the B_{ay} and the additional induced magnetic moment can be avoided. The m_y can be measured based on

$$\bar{\tau}_z = B_{cx} m_y \sin(\omega t), \tag{6}$$

where the $\bar{\tau}_z$ are measured by a precision torsion pendulum.

III. EXPERIMENTAL INSTRUMENT

Our torsion pendulum apparatus has been specifically designed to investigate magnetic properties and electrostatic related effects [19,21]. A schematic of our core instrument is shown in Fig. 2. The pendulum is a cube-shaped copper TM suspended by a 60 cm long, 125 μm diameter, W fiber. The TM is constituted by a 5-cm-side cubical-shaped copper (99.9999% purity, T6), and a reflector used for optical readout of the pendulum rotational angle is located at the center of one side of the TM. The pendulum body twist $\theta(t)$ is monitored by an autocollimator that reflects the light off the reflector. The coil dimensions and position are shown in Fig. 1. The 2D

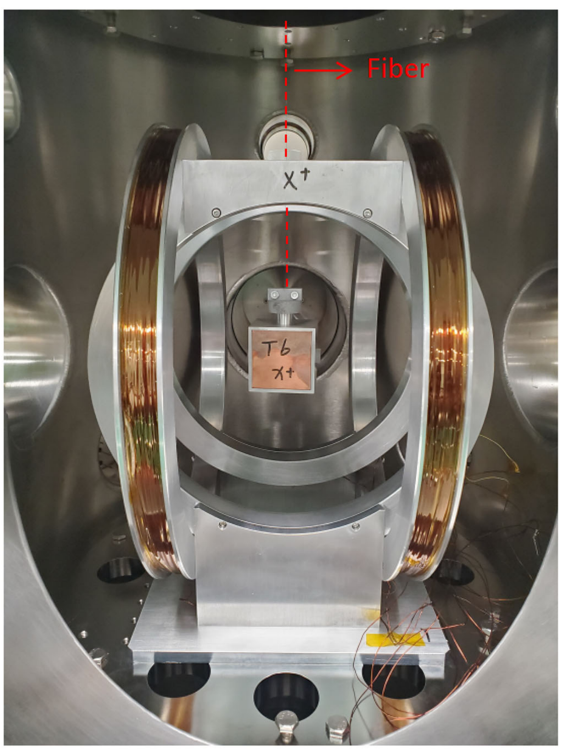

FIG. 2. Schematic diagram of the instrument.

Helmholtz coils field uniformity in TM space along the x-axis and y-axis are 2.7% and 1.5% respectively. The torsion pendulum and the 2D Helmholtz coils are installed in vacuum chamber maintained at a pressure of 10^{-5} Pa.

The free oscillation period T_0 of the torsion pendulum, with calculated moment of inertia $I=4.6\times10^{-4}$ kg m^2, is 72 s. Then, the equation of motion of the pendulum can be written as $I\ddot{\theta}+\beta\dot{\theta}+k\theta=\bar{\tau}_z+\tau_{th}$, where $k=4\pi^2 I/T_0^2$ is the elastic constant of fiber. The $\bar{\tau}_z$ and τ_{th} are torque produced by the magnetic field and the thermal fluctuation separately.

The $\beta=\frac{kT_0}{2\pi Q}$ is the dissipative term of the torsion pendulum, where Q is the quality factor of the torsion pendulum system [22]. It can be expressed as [23]

$$\frac{1}{Q}=\frac{1}{Q_{\mathrm{mag}}}+\sum\frac{1}{Q_{\mathrm{other}}}, \tag{7}$$

where $1/Q_{\mathrm{mag}}$ is the eddy current dissipation due to motion of the TM in the magnetic field $B_{ay}+B_{cy}$, $1/Q_{\mathrm{other}}$ are the other loss terms such as the intrinsic structural damping and the gas damping and so on.

IV. MEASUREMENT AND RESULTS

Based on experimental principle in Eq. (5), the zero field environment $B_{ay}+B_{cy}=0$ should be achieved before the formal experiment. We perform modulation experiments of B_{cy} to measure the B_{ay} based on the relation [24]: $\frac{1}{Q}\propto\frac{1}{Q_{\mathrm{mag}}}\propto(B_{ay}+B_{cy})^2$. In Eq. (7), when actual field $B_{ay}+B_{cy}$ changes, the Q_{mag} and later Q will alter, and the Q reach its maximum with a zero field ($B_{ay}+B_{cy}=0$) along the y-axis. For constant of the Q_{other}, the initial amplitude of torsion pendulum and the ambient temperature are maintained same [25]. The typical amplitude attenuation of torsion pendulum under two modulated fields B_{cy} are shown in Fig. 3. The measuring method of the Q is the conventional amplitude attenuation method [26].

By modulation of the B_{cy} produced by y-axis coil of 2D Helmholtz coils, the relation of Q and B_{cy} can be given in the Fig. 4. The 13 series data of the Q with modulated B_{cy} are fitted with a quadratic function model [27]. The zero field can be reached with the modulated $B_{cy}=-(33.34\pm0.04)$ μT.

In measurements of the m_y, the modulated $B_{cy}=-B_{ay}$ is maintained to compensate the ambient field component B_{ay}. In this way, the superimposed magnetic field $B_{cy}+B_{ay}$ approximates to zero are acquired.

The amplitude of modulated field B_{cx} is set to (360 ± 0.02) μT, and the ω are swept 1–20 mHz. The frequency sweep operations are used to guarantee the zero field. If not, according to Eq. (5), the amplitude of the torque $\bar{\tau}_z$ is frequency dependent. The results of two modulated cycles are shown in Fig. 5. The linear correlation

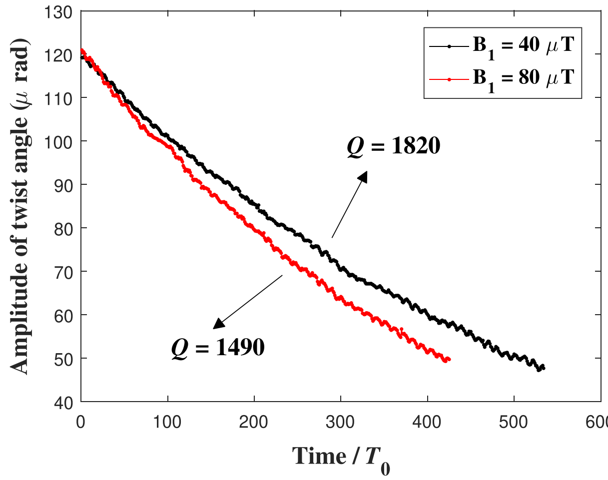

FIG. 3. The typical amplitude attenuation of the twist angle of the torsion pendulum for different modulated values of B_{cy}. The abscissa is the normalized time (actual time divided by period T_0). The ordinate represents the amplitude of the twist angle at the normalized time. The black and red dots are the amplitude attenuation under modulated $B_{cy} = 40\ \mu\mathrm{T}$ and $B_{cy} = 80\ \mu\mathrm{T}$ respectively.

coefficients between the torque $\bar{\tau}_z$ and frequency ω in two cycles are 0.08 and 0.13 separately. It implies the B_{ay} is compensated satisfactorily, and the zero field along the y-axis is constructed. Since the coincidence of $\bar{\tau}_z$ in two cycles, all $\bar{\tau}_z$ data are adopted with weighted average method [28], and the amplitude of torque $\bar{\tau}_z$ is estimated as (5.33 ± 0.06) pN m. The errors of m are fully evaluated in Table I. The constant systematic relative error is about

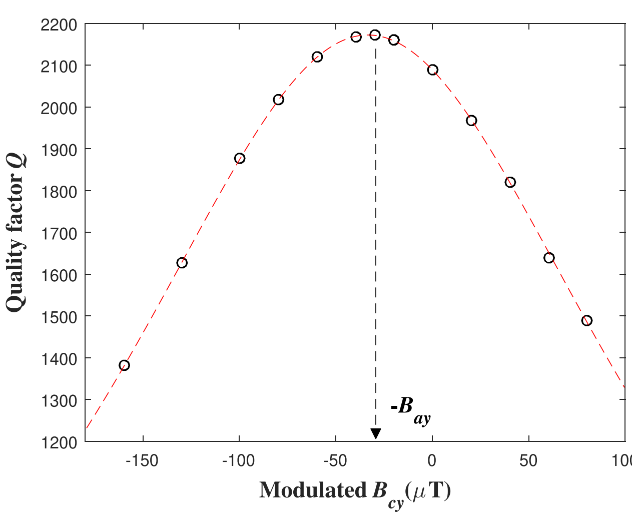

FIG. 4. The relation of the Q and the modulated B_{cy}. The hollow black dots are the measured values under the different modulated field B_{cy}. The red line marks the fitting of the modulated B_{cy} and Q with a quadratic function model. Since the tiny measured errors of B_{cy} and Q are $0.02\ \mu\mathrm{T}$ and ~ 5 respectively, the error bars are not drawn.

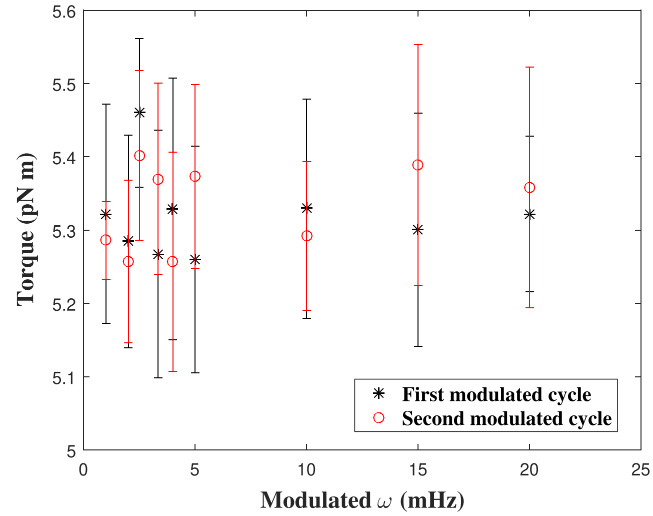

FIG. 5. The torques $\bar{\tau}_z$ with different modulated frequency in two cycles. The asterisks and their error bars (3σ) represent the results in the first cycle. The circles and their error bars represent the results in the second cycle.

1.5% mainly due to the imperfect uniformity of the field B_{cx}. The statistical relative error 1.2% is calculated in data processing of the $\bar{\tau}_z$. According to Eq. (6), the m_y is measured as $-[14.80 \pm 0.22(\mathrm{sys}) \pm 0.17(\mathrm{stat})]\ \mathrm{nA\,m^2}$. The symbol negative sign expresses the direction of m_y reverse the y axis.

The processes of measurement of m_x are the same as those for m_y. The coils along the x axis are used to measure and compensate the ambient field B_{ax}. The measured B_{ax} is $(22.50 \pm 0.04)\ \mu\mathrm{T}$. The coils along the y axis are used to modulate field to measure the m_x. We measured $m_x = [37.67 \pm 1.02(\mathrm{sys}) \pm 0.44(\mathrm{stat})]\ \mathrm{nA\,m^2}$, here the systematic relative error is larger than that of m_y since the larger uniformity of the coil along the y. By revolving the TM 90 degrees (clockwise) around x-axis, the m_z and m_x can be measured as $[8.41 \pm 0.13(\mathrm{sys}) \pm 0.11(\mathrm{stat})]$ and $[37.92 \pm 0.56(\mathrm{sys}) \pm 0.45(\mathrm{stat})]\ \mathrm{nA\,m^2}$ with the same processes, respectively. The results of the m_x before and after the revolution are coincident under 1σ error bar.

TABLE I. One σ uncertainty budget (in units of 10^{-2}).

Error sources	$\Delta m_y/m_y$
Uniformity of B_{cx}	1.5
Residual B_{ax}	<0.01
Moment of inertia I	<0.03
Free oscillation period T_0	0.01
Combined systemic relative error	1.51
Fluctuation of torque $\bar{\tau}_z$	1.2
Fluctuation of Q	<0.3
Combined statistic relative error	1.23
Total	1.95

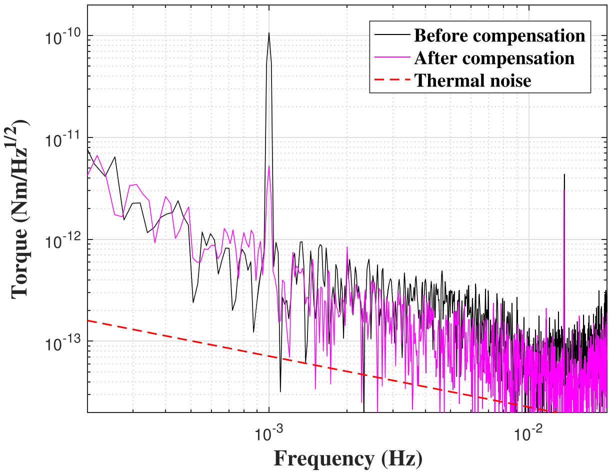

FIG. 6. The amplitude spectral density of torques of the torsion pendulum. The black and pink lines mark the torques before and after the compensation of the B_{ay} respectively. The modulating signal is observed at 1 mHz.

It indicates that the measurement system is stable, even though the torsion pendulum may swing significantly during the operation of reversing the test mass. The compounded $|m|$ of TM equals $[41.56 \pm 0.62(\mathrm{sys}) \pm 0.50(\mathrm{stat})]$ nA m^2 with the precision better than 1 nA m^2.

V. DISCUSSION

In this measurement, the ambient magnetic field should be compensated in torsion pendulum experiment with the modulated AC magnetic field to measure the m of TM. We contrast the experiment results before and after ambient magnetic field B_{ay} compensated. As Fig. 6 shows, two modulated experiments are performed at 1 mHz. The measured torques before and after the compensation are about 100 pN m$/\sqrt{\mathrm{Hz}}$ and 5 pN m$/\sqrt{\mathrm{Hz}}$ respectively. The major torque contribution comes from the additional induced magnetic moment coupling with the B_{ay}. This torque due to the non uniformity of the susceptibility is much larger than the torque due to the field non-uniformity. The measurement of the m will be exceeded about 20 times in case of the uncompensated B_{ay} in previous method [8]. In previous experiments, the modulated DC magnetic fields were applied to measure the m, namely, the $\omega = 0$ in Eq. (5) [11,12,14]. The measured deviation still exists due to the potential induced anisotropy [29]: $\chi_x(0) - \chi_y(0) \neq 0$. We cannot verify the anisotropy since some complicated torque noise such as the temperature gradients and the radiometer effect will apply to the torsion pendulum in $\omega = 0$ condition [30]. However, whether the anisotropy exists or not, the influence of the anisotropy can be suppressed by the compensation of the ambient field.

To avoid the potential complicated torque noise in $\omega = 0$ condition, we consider the modulated AC magnetic field method proposed by Hueller *et al.* can separate the targeted magnetic torque from these noises in frequency domain clearly. That is why we adopt the modulated field to measure the m after the compensation of ambient field.

In TianQin GW detection mission, since the magnetic acceleration noises are proportional to the component of the m along the sensitive axis of GW detection. Based on the precision measurement of $m = (m_x, m_y, m_z)$, one can choose the smaller component for the smaller residual acceleration before the machining and cutting of TM [31]. For instance, since the contribution noise ratio of our mimic TM is 5:2:1 while adopting the x, y, z as the sensitive axes respectively, the z axis should be chosen. This means that before further overall processing (gilding, gripping positioning, and release mechanism) of the TM, the sensitive axis of the TM can be optimized based on measurement results of (m_x, m_y, m_z) for suppressing the magnetic noise.

VI. SUMMARY

In this work, the magnetic moment m components are measured at 1 nA m^2 precision level by the torsion pendulum with the modulated 2D Helmholtz coils for TianQin GW detection mission. The measurements are not depending on the assumption of the uniform distribution of m in TM volume. The undesired significant interference due to the ambient magnetic field is avoided by the design of compensation. Our work provides a precise method for measuring the remanent magnetic moment of TM applied in space GW detection missions. As a precision torque magnetometer, it is helpful in assessing the applicability of the large mass weakly magnetic samples for various scientific and engineering applications.

ACKNOWLEDGMENTS

We are very appreciative of an anonymous reviewer for important comments. This work is supported by the National Key R&D Program of China (Grant No. 2020YFC2200500), the Key Laboratory of TianQin Project (Sun Yat-sen University), Ministry of Education, the National Natural Science Foundation of China (Grants No. 12075325, No. 12005308, and No. 11605065).

[1] C. F. Everitt, D. DeBra, B. Parkinson, J. Turneaure, J. Conklin, M. Heifetz, G. Keiser, A. Silbergleit, T. Holmes, J. Kolodziejczak *et al.*, Gravity probe B: Final results of a space experiment to test general relativity, Phys. Rev. Lett. **106**, 221101 (2011).

[2] J. Conklin, S. Buchman, V. Aguero, A. Alfauwaz, A. Aljadaan, M. Almajed, H. Altwaijry, T. Al-Saud, K. Balakrishnan, R. Byer *et al.*, LAGRANGE: LAser GRavitational-wave ANtenna at Geo-lunar Lagrange points, arXiv:1111.5264.

[3] B. R. Patla, Reduction of magnetic perturbation for SR-POEM, Classical Quantum Gravity **33**, 045006 (2016).

[4] P. Touboul, G. Métris, M. Rodrigues, Y. André, Q. Baghi, J. Bergé, D. Boulanger, S. Bremer, P. Carle, R. Chhun *et al.*, Microscope mission: First results of a space test of the equivalence principle, Phys. Rev. Lett. **119**, 231101 (2017).

[5] B. Frommknecht, Integrated sensor analysis of the GRACE mission, Ph.D. thesis, Technische Universität München, 2007.

[6] P. Amaro-Seoane, H. Audley, S. Babak, J. Baker, E. Barausse, P. Bender, E. Berti, P. Binetruy, M. Born, D. Bortoluzzi *et al.*, Laser interferometer space antenna, arXiv:1702.00786.

[7] J. Luo, L.-S. Chen, H.-Z. Duan, Y.-G. Gong, S. Hu, J. Ji, Q. Liu, J. Mei, V. Milyukov, M. Sazhin *et al.*, TianQin: A space-borne gravitational wave detector, Classical Quantum Gravity **33**, 035010 (2016).

[8] M. Hueller, M. Armano, L. Carbone, A. Cavalleri, R. Dolesi, C. Hoyle, S. Vitale, and W. Weber, Measuring the LISA test mass magnetic properties with a torsion pendulum, Classical Quantum Gravity **22**, S521 (2005).

[9] L. Zaragoza, Magnetically induced forces during LISA Pathfinder in-flight operations, Ph.D. thesis, Universitat autónoma de Barcelona, 2020.

[10] W. Su, Y. Wang, Z.-B. Zhou, Y.-Z. Bai, Y. Guo, C. Zhou, T. Lee, M. Wang, M.-Y. Zhou, T. Shi *et al.*, Analyses of residual accelerations for TianQin based on the global MHD simulation, Classical Quantum Gravity **37**, 185017 (2020).

[11] T. Hai-Bo, B. Yan-Zheng, Z. Ze-Bing, L. Yu-Rong, and L. Jun, Measurement of magnetic properties of an inertial sensor with a torsion balance, Chin. Phys. Lett. **26**, 040403 (2009).

[12] H. Yin, D.-Y. Tan, M. Hu, S. Wang, Y.-Z. Bai, S.-C. Wu, and Z.-B. Zhou, Measurements of magnetic properties of kilogram-level test masses for gravitational-wave detection using a torsion pendulum, Phys. Rev. Appl. **15**, 014008 (2021).

[13] M.-N. Qiao, L.-H. Liu, B.-S. Cai, Y.-T. Zhang, Q.-L. Wang, J.-H. Xu, and Q. Liu, Measurement of remanent magnetic moment using a torsion pendulum with single frequency modulation method, Chin. Phys. B **32**, 050702 (2023).

[14] B. Liu, Z. Yang, L.-e. Qiang, P. Xu, X. Peng, Z. Luo, Y. Zhang, and W. Tang, An improved magnetic properties measurement scheme using a torsion pendulum, Results Phys. **54**, 107048 (2023).

[15] M. Schaapman, P. Christianen, J. Maan, D. Reuter, and A. Wieck, A multipurpose torsional magnetometer with optical detection, Appl. Phys. Lett. **81**, 1041 (2002).

[16] F. Constant, Ferromagnetic impurities in metals, Rev. Mod. Phys. **17**, 81 (1945).

[17] R. S. Davis, Determining the magnetic properties of 1 kg mass standards, J. Res. Natl. Inst. Stand. Technol. **100**, 209 (1995).

[18] M. Weber, R. Koch, and K. Rieder, UHV cantilever beam technique for quantitative measurements of magnetization, magnetostriction, and intrinsic stress of ultrathin magnetic films, Phys. Rev. Lett. **73**, 1166 (1994).

[19] J.-H. Xu, Q. Liu, X. Luo, L. Zhu, H.-H. Zhao, Q.-L. Wang, S.-Q. Yang, J. Luo, Measuring ac magnetic susceptibility at low frequencies with a torsion pendulum for gravitational-wave detection, Phys. Rev. Appl. **18**, 044010 (2022).

[20] L. D. Landau, J. S. Bell, M. Kearsley, L. Pitaevskii, E. Lifshitz, and J. Sykes, *Electrodynamics of Continuous Media* (Elsevier, New York, 2013), Vol. 8.

[21] X. Pi, Q. Liu, J. Xu, L. Zhu, Q. Wang, Y. Zhang, S. Yang, and J. Luo, Continuous charge management scheme for Tianqin, Classical Quantum Gravity **40**, 035005 (2023).

[22] G. Russano, A torsion pendulum ground test of the LISA Pathfinder free-fall mode, arXiv:1609.00002.

[23] T. Uchiyama, T. Tomaru, M. Tobar, D. Tatsumi, S. Miyoki, M. Ohashi, K. Kuroda, T. Suzuki, N. Sato, T. Haruyama *et al.*, Mechanical quality factor of a cryogenic sapphire test mass for gravitational wave detectors, Phys. Lett. A **261**, 5 (1999).

[24] V. B. Braginsky and A. B. Manukin, *Measurement of Weak Forces in Physics Experiments* (University of Chicago Press, Chicago, 1977).

[25] Z.-K. Hu and J. Luo, Amplitude dependence of quality factor of the torsion pendulum, Phys. Lett. A **268**, 255 (2000).

[26] C. Hagedorn, S. Schlamminger, and J. Gundlach, Quality factors of bare and metal-coated quartz and fused silica torsion fibers, AIP Conf. Proc. **873**, 189 (2006).

[27] D.-H. Wang, X.-l. Wang, L. Zhao, and L.-c. Tu, Eddy current loss testing in the torsion pendulum, Phys. Lett. A **290**, 41 (2001).

[28] D.-H. Wang, J. Luo, and K. Luo, Precise determination of the amplitude of signal with known frequency based on correlated noise model, Rev. Sci. Instrum. **77**, 104501 (2006).

[29] U. Gradmann, W. Kümmerle, and R. Tham, High sensitivity torsion magnetometers for oligatomic films, Appl. Phys. **10**, 219 (1976).

[30] S. E. Pollack, S. Schlamminger, and J. H. Gundlach, Outgassing, temperature gradients and the radiometer effect in LISA: A torsion pendulum investigation, AIP Conf. Proc. **873**, 158 (2006).

[31] F. Antonucci, M. Armano, H. Audley, G. Auger, M. Benedetti, P. Binetruy, C. Boatella, J. Bogenstahl, D. Bortoluzzi, P. Bosetti *et al.*, LISA Pathfinder: Mission and status, Classical Quantum Gravity **28**, 094001 (2011).